SvedbergOpen
DISSEMINATION OF KNOWLEDGE

International Journal of Artificial Intelligence and Machine Learning

Publisher's Home Page: https://www.svedbergopen.com/

Research Paper Open Access

# Simulation and Experimental Validation of Reinforcement Learning-Based Adaptive Sliding Mode Control for a Flexible-Joint Robotic Manipulator

Hayder Z. Abdalkhwa[1], Waleed Al-Ashtari[2]

[1] Mechanical Engineering Department, College of Engineering, University of Baghdad, Baghdad 10071, Iraq.
E-mail: haidar.zaher2303@coeng.uobaghdad.edu.iq
[2] Engineering Applications Department, College of Artificial Intelligence, University of Baghdad, Baghdad 10071, Iraq.
E-mail: waleed.al.ashtari@coeng.uobaghdad.edu.iq

**Abstract**

In this work, an adaptive sliding mode controller (ASMC) for a flexible-joint robotic manipulator using reinforcement learning is presented and validated by experiments and simulations. The control strategy has been designed to be implemented on a practical platform, which has been designed and fabricated as a four-degree-of-freedom robotic manipulator equipped with a flexible joint. RL-ASMC combines reinforcement learning and Adaptive Sliding Mode Control (ASMC) to adapt the parameters of the controller and improve the position tracking performance under different operating conditions. The non-linear robotic system and control algorithms were simulated in MATLAB/Simulink and real-time implementation of the control system was programmed in LabVIEW/ NI myRIO for the fabricated Robotic Platform. The same external disturbances, no load and payload were applied to ASMC and RL-ASMC. The key performance measures used were angular position error, settling time, the maximum estimated control torque, and disturbance rejection. Experimental results demonstrated that the performance of RL-ASMC is superior to the standalone ASMC, which decreases the angular position error about 71%, settling time about 16%, and the maximum estimated control torque about 10%, respectively. Moreover, the simulated and experimental results were found to be in good agreement, with the average deviations of 4.8% and 4.3% for ASMC and RL-ASMC at the reference angles of 135° and 45°, respectively. The results show the effectiveness, stability, and usability of RL-ASMC for the robotic manipulators with flexible joints.

**Keywords:** Flexible-joint robotic manipulator; Adaptive sliding mode control; Reinforcement learning; Experimental validation; Four-spring elastic joint; LabVIEW; NI myRIO.

## 1. Introduction

In recent years, a flexible-joint robotic manipulator has been gaining increasing attention in various fields of robotics due to the benefits that can be gained from mechanical compliance, such as impact absorption, safe interaction, structural protection, and adaptability to wide range of working environments. But the elasticity of joints imposes extra nonlinear dynamics, elastic oscillations, motor–load coupling, and parameter uncertainty, payload variation, and external disturbance sensitivity on the system when compared to traditional systems with rigid joints. These features significantly make it more difficult to obtain accurate and stable position tracking. Thus, many studies have been dedicated to the modeling and control design of flexible-joint robotic manipulators, such as adaptive control, robust control, prescribed-performance control, passivity-based control, model predictive control and intelligent control [1-8].

Sliding Mode Control (SMC) is one of the most popular and effective nonlinear control methods due to its excellent model uncertainty and external disturbance rejection performance [9–12]. However, the abrupt switching behavior of conventional SMC can introduce chattering into the system resulting in undesirable oscillations and control effort in real robotic systems. There have been several modified sliding mode approaches, therefore, proposed to guarantee convergence and eliminate chattering in flexible-joint manipulators [9-13]. One such solution is Adaptive Sliding Mode Control (ASMC) which incorporates a variable controller gain based on the behavior of the system. This adaptive capability can help to keep the system robust even though operating conditions shift [12–16].

In recent years, flexible-joint robot control has evolved to increasingly incorporate adaptive, neural, optimization and learning approaches to deal with uncertainties that are hard to be accurately represented by fixed mathematical models [2–5, 14–18]. Adaptive neural and prescribed-performance controllers have been shown to provide superior tracking performance in the presence of dynamic uncertainties and under input constraints [2–8] and hybrid and optimization-based controllers have been shown to perform better when the model parameters change, such as joint stiffness, payload, and external disturbances [14–18]. Advanced adaptive and sliding mode controllers have also been demonstrated to yield good tracking and disturbance rejection performance in case of physical flexible-joint systems [12, 16–19]. These developments reflect a gradual trend toward a model-free robust control approach and to architectures for intelligent control with parameter adaptation based on the system behavior. The incorporation of such learning power has been achieved by using Reinforcement Learning (RL) in the control system of the robots [20-23]. While a fixed set of parameters for the controller is not used in RL, a control policy or controller parameters can be dynamically adjusted according to the actual response from the system and a specified performance goal. This is especially true of flexible-joint manipulators, where the effective dynamics might change depending on payload, flexibility of the joints, and disturbances. Recently, Pavlichenko and Behnke [22] demonstrated the effectiveness of deep reinforcement learning for improving the position tracking performance of a real Baxter with flexible joints, which has 7 degrees of freedom. Their learning-based reference-correction approach enhanced the tracking performance and established good generalizability to an unknown payload, supporting the transfer of RL from a numerical environment to a physical flexible-joint robotic system. Recently, Zhong et al. [23] have proposed a reinforcement-learning based adaptive tracking control for the flexible-joint robotic manipulators. They solved the Hamilton–Jacobi–Bellman equation coupled with an optimal control method in a backstepping manner with an actor–critic neural network architecture.

The performance index incorporated both tracking error and control input, allowing tracking performance and control effort to be considered simultaneously. The effectiveness of the method was demonstrated through numerical simulations of a flexible-joint robotic system. This study represents an important development in learning-based flexible-joint control; however, the proposed architecture was based on optimal backstepping and its evaluation was simulation-based rather than a direct experimental comparison between conventional adaptive sliding-mode control and its reinforcement-learning-enhanced counterpart.

Other recent studies have continued to advance flexible-joint control through disturbance observers, safety-constrained model predictive control, elastic-structure-preserving control, neural adaptation, and hybrid optimization techniques [17–19, 24–27]. Collectively, these studies demonstrate substantial progress in tracking accuracy, vibration suppression, robustness, and disturbance rejection. Nevertheless, the literature indicates that comparatively limited attention has been devoted to determining the specific improvement obtained by incorporating reinforcement-learning-based parameter adaptation into ASMC and verifying whether the resulting improvement observed in simulation is preserved during real-time experimental implementation. This issue is particularly important because physical robotic systems contain actuator dynamics, sensor effects, mechanical elasticity, payload variations, and unmodeled disturbances that cannot always be completely represented in simulation.

To address this issue, the present study develops a Reinforcement Learning-Based Adaptive Sliding Mode Controller (RL-ASMC) for a four-degree-of-freedom flexible-joint robotic manipulator. A robotic manipulator incorporating a flexible joint was designed and fabricated to provide a physical platform for real-time controller evaluation. The nonlinear robotic system and control algorithms were investigated through MATLAB/Simulink, whereas the experimental control system was implemented using LabVIEW and NI myRIO. To isolate and quantify the contribution of reinforcement learning, the proposed RL-ASMC is directly compared with standalone ASMC under identical no-load, payload, and external-disturbance conditions.

The comparison considers angular position tracking error, settling time, maximum estimated control torque, and disturbance-rejection capability. In addition, corresponding simulation and experimental results are quantitatively compared to determine the consistency between the numerical model and the physical robotic system.

The main contributions of this study are: (1) integration of reinforcement-learning-based parameter adaptation with ASMC for position control of a flexible-joint robotic manipulator; (2) implementation and evaluation of the proposed RL-ASMC on a designed and fabricated 4-DOF flexible-joint robotic platform; (3) direct quantitative comparison between ASMC and RL-ASMC under identical operating conditions to determine the performance improvement attributable specifically to reinforcement learning; and (4) direct validation of MATLAB/Simulink predictions against real-time LabVIEW/NI-myRIO experimental results under no-load, payload, and external-disturbance conditions.

### 1.1 Significance of the Study

This study demonstrates the practical significance of integrating reinforcement learning with adaptive sliding mode control for flexible-joint robotic manipulators. The proposed RL-ASMC provides an intelligent mechanism for real-time tuning of the controller parameters according to changes in operating conditions. The experimental validation on a fabricated 4-DOF robotic platform confirms that the proposed approach can improve position tracking accuracy, response speed, disturbance rejection, and control efficiency. Therefore, the study provides a practical contribution toward the development of more adaptive and robust control systems for flexible-joint robotic manipulators.

## 2. Materials and Methods

### 2.1 Flexible-Joint Robotic Manipulator

A 4-DOF robotic manipulator incorporating a flexible joint was designed and fabricated as the experimental platform for this study. The manipulator consists of four actuated joints, with an elastic coupling introduced at one joint between the motor side and the load side. The mechanical configuration was initially developed using SolidWorks and subsequently manufactured and assembled to enable real-time implementation and experimental validation of the proposed control strategies as shown in figure 1

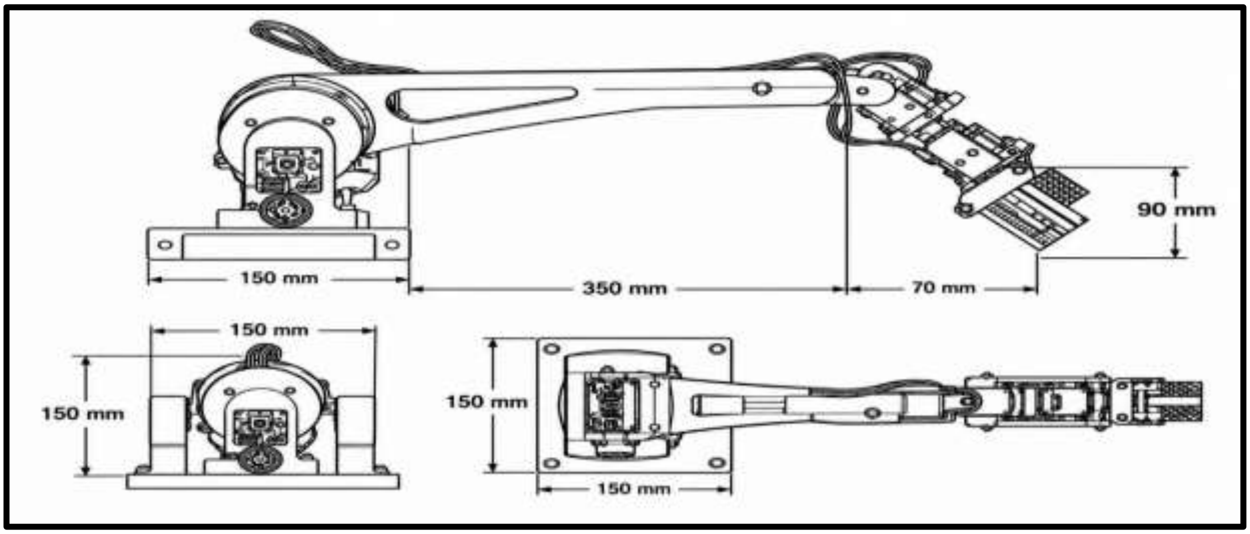


**Figure 1.** Schematic of the 4-DOF flexible-joint robotic manipulator

The flexible joint follows the principle of a Series Elastic Actuator (SEA), in which an elastic element is intentionally introduced between the actuator and the driven load. Consequently, the motor torque is transmitted to the load through the compliant element rather than through a completely rigid connection. Such mechanical compliance provides several advantages, including shock absorption, vibration isolation, reduction of mechanical stresses transmitted to the actuator and transmission components, and improved operational safety. However, the introduced elasticity also produces relative angular displacement between the motor and load sides and may generate oscillatory behavior, thereby increasing the difficulty of accurate position control [1,2].

In the developed manipulator, the flexible joint is represented by two coupled rotational coordinates: the motor-side angular position, $\theta m$, and the load-side angular position, $\theta l$. Their relative angular displacement,

$\theta = \theta m - \theta l$ ................................ (1)

represents the elastic deformation of the flexible joint and determines the restoring torque transmitted between the motor and load sides. This configuration provides an appropriate physical platform for investigating controller performance under joint elasticity, payload variation, and externally applied disturbances.

The fabricated manipulator was used for the experimental implementation of both ASMC and RL-ASMC, allowing their performance to be evaluated under the same mechanical and operating conditions. This also enables a direct comparison between the numerical model developed in MATLAB/Simulink and the real-time experimental system implemented through LabVIEW and NI myRIO.

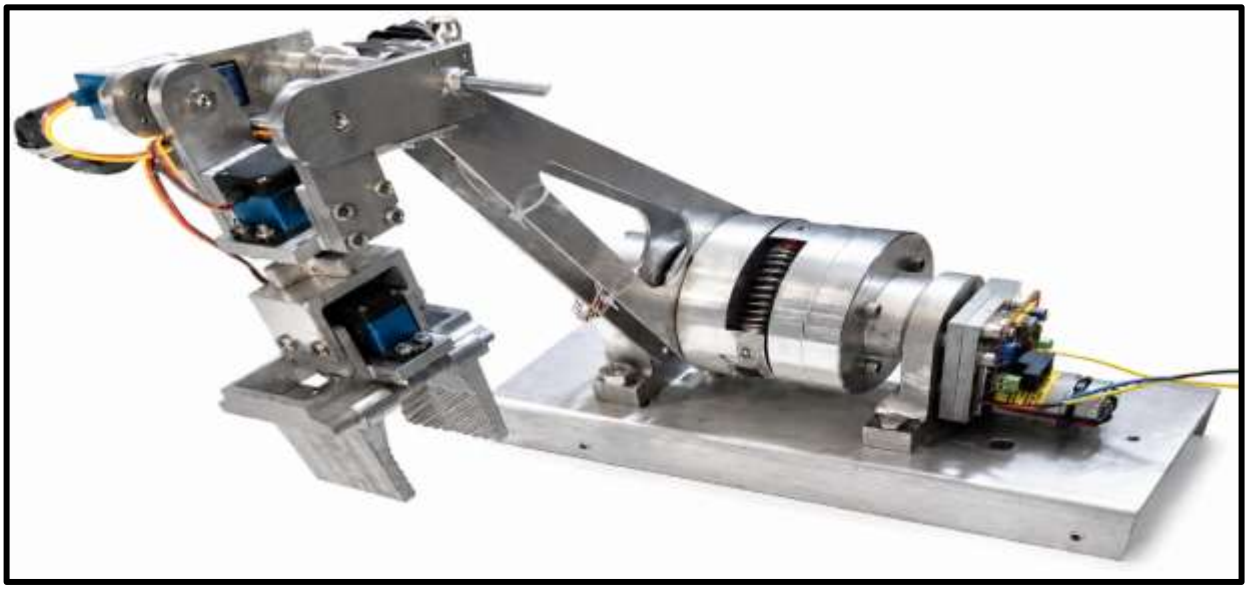

**Figure 2.** Developed 4-DOF robotic manipulator with a flexible joint

**2.2 Flexible-Joint Mechanism and Mathematical Model**

The flexible steel joint consists of a 140 mm diameter cylindrical frame composed of two main parts. The first part is connected to the main motor, while the second part is connected to the first load-side arm. Four identical springs are symmetrically mounted around the circular frame between these two parts, as shown in Figure 3. The flexible-joint mechanism was designed using SolidWorks and subsequently fabricated for experimental implementation.

The proposed design provides torsional flexibility, thereby protecting the motor from high loads and absorbing sudden shocks during operation. The flexible coupling also permits relative angular displacement between the motor and load sides, introducing elastic characteristics and a phase delay that influence the dynamic response of the robotic manipulator

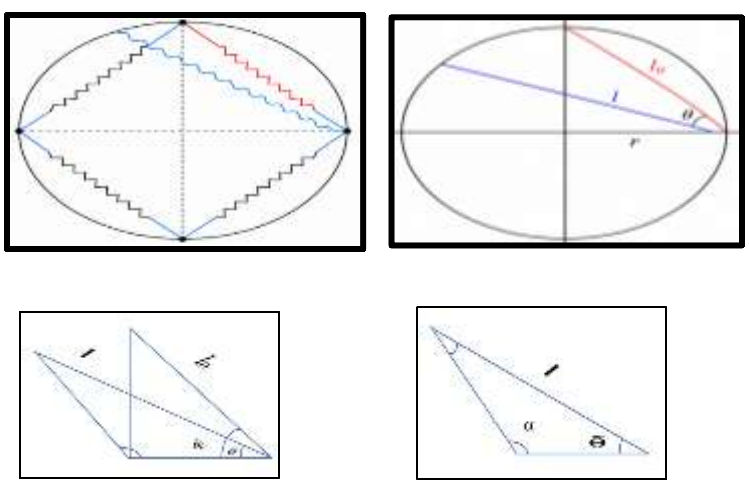

**Figure 3.** Schematic of the flexible joint

The relative angular displacement between the motor and load sides, previously introduced in Section 2.1, is expressed as:

$\theta = \theta m - \theta l$ ................................ (1)

The four springs are symmetrically distributed around the flexible joint and are assumed to have identical stiffness coefficients:

$K_1=K_2=K_3=K_4 = K$ ................................ (2)

For the geometrical configuration of the proposed joint, the initial spring angle is
$\theta_0 = \pi/4$ ………………...(3)
The angular deflection of the flexible joint is defined as follows:
$\tilde{\theta} = \theta_0 - \theta$ ………………...(4)
where θ is the angular deformation and $\tilde{\theta}$ is the remaining geometric angle.
Based on the geometry of the spring arrangement, the initial spring length is
At the initial position, the two radii form a right angle. Hence, the initial spring length is
$l_0 = \sqrt{2}\, r$ …………………………….. (5)
where is the radial distance from the joint center to the spring attachment point. After angular displacement, the spring length becomes
$l = \sqrt{2}\, r \sqrt{(1 - \cos(\alpha))}$ …………………………….. (6)
Hence, the spring elongation is
$\Delta = l - l_0 = \Delta = \sqrt{2}\, r\, [\sqrt{(1 + \sin(2\theta))} - 1]$ ……………………. (7)
Using Hooke's law, the spring force is
$F = K\Delta$ …………………………….. (8)
The perpendicular moment arm of the spring force is
$R = r \sin(\tilde{\theta})$ …………………………….. (9)
Therefore, the restoring torque generated by a single spring is
$T_s = RF$ …………………………….. (10)
Substituting the spring force and elongation expressions gives
$T_s = \sqrt{2}\, r^2 K \sin(\tilde{\theta})[\sqrt{(1 + \sin(2\theta))} - 1]$ …………… (11)
Since the flexible joint contains four identical and symmetrically arranged springs, the total restoring torque is
$Tfj = 4\sqrt{2}\, r^2 K \sin(\tilde{\theta})[\sqrt{(1 + \sin(2\theta))} - 1]$ ………… (12)
The generalised coordinate vector of the comprehensive flexible-joint robotic system is defined as:
$q = [\theta_m\ \theta_1\ \ \theta_2\ \theta_3]^T$ …………………..(13)
$q$ : generalized joint-angle vector of the proposed flexible-joint robotic arm.
$\theta_m$ denotes the motor-side angle of the flexible joint, while $\theta_m\ \ \theta_1\ \ \theta_2$ and $\theta_3$
specify the angular orientations of the remaining joints of the robotic arm.
Using the Euler–Lagrange formulation, the nonlinear dynamic model of the robotic manipulator can be expressed as
$\boldsymbol{M(q)\ddot{q} + H(q,\dot{q}) + G(q) = Q}$ **………………(14)**
$M(q)$: is the inertia matrix, $H(q,\dot{q})$: velocity coupling vector, $G(q)$: gravitational force vector, and $Q_i$: generalized torque vector.
The nonlinear torque produced by the flexible joint is introduced into the generalized torque vector through
$Q = \tau_a + B_j T_s$ ………………(15)
where denotes the actuator torque vector and the flexible-joint torque distribution vector is
$B_j = [\,-1\ \ 1\ \ 0\ \ 0\,]^T$ …………………...(16)
he negative and positive signs indicate the opposite action of the internal flexible-joint torque on the motor-side and first load-side coordinates, respectively. Substituting Eq. (15) into Eq. (14) yields the coupled nonlinear dynamic model of the developed flexible-joint robotic manipulator:
$\boldsymbol{M(q)\ddot{q} + H(q,\dot{q}) + G(q) = \tau_a + B_j T_s}$ **………………(17)**

### 2.3 Controller Design

#### 2.3.1 Adaptive Sliding Mode Controller (ASMC)

To achieve accurate position tracking in the presence of the nonlinear flexible-joint dynamics, payload variations, and external disturbances, an Adaptive Sliding Mode Controller (ASMC) is employed. The tracking error is defined as the difference between the desired and actual joint-position vectors:
$e(t) = q_d(t) - q(t)$, ……………...(18)
where:
$q_d(t)$ : the desired joint trajectory vector, and $q(t)$ : the actual joint position vector
The sliding surface is delineated as follows [28]:
$S(t) = \dot{e}(t) + \Lambda e(t)$ …………….............(19)
$S(t)$:is the sliding surface vector.
where Λ is a positive diagonal matrix that determines the convergence rate of the tracking error.
To reduce the chattering associated with the discontinuous switching action of conventional SMC, a continuous hyperbolic tangent function is employed. The adaptive switching component is expressed as
$u_{sw} = -\eta(t) \tanh\left(\frac{S}{\emptyset}\right)$ ………………… (20)
where: η(t): is a time-varying adaptive switching gain,Ø: is the boundary Layer Thickness parameter, Ø >0

the ASMC control law is written as:

$$\boldsymbol{u = u_{eq} - \eta(t)\ \tanh\left(\frac{S}{\emptyset}\right)} \quad \text{………………} \ \textbf{(21)}$$

where $\boldsymbol{u_{eq}}$ denotes the equivalent control component.

The switching gain is continuously adjusted according to the magnitude of the sliding variable using the adaptive law

$$\dot{\eta} = \gamma\ |S| \qquad \text{…………………(22)}$$

where $\gamma > 0$ represents the adaptation gain that dictates the rate of gain modification.

his adaptive mechanism allows the switching gain to increase according to the tracking condition instead of relying on a fixed, conservatively selected gain, thereby maintaining robustness against uncertainties and disturbances while reducing excessive switching action.

For stability analysis, the following Lyapunov candidate function is considered:

$$\boldsymbol{V = \frac{1}{2}\ S^T S\ + \frac{1}{2\gamma}\,(\eta - \eta^*)^2} \quad \text{…………………………}\textbf{(23)}$$

By applying the adaptive law in Eq. (21) and appropriately selecting the controller parameters, the time derivative of the Lyapunov function satisfies the required stability condition, ensuring convergence of the sliding variable toward the sliding surface and maintaining closed-loop stability.

The overall structure of the proposed ASMC and its interaction with the flexible-joint robotic manipulator are illustrated in figure 4.

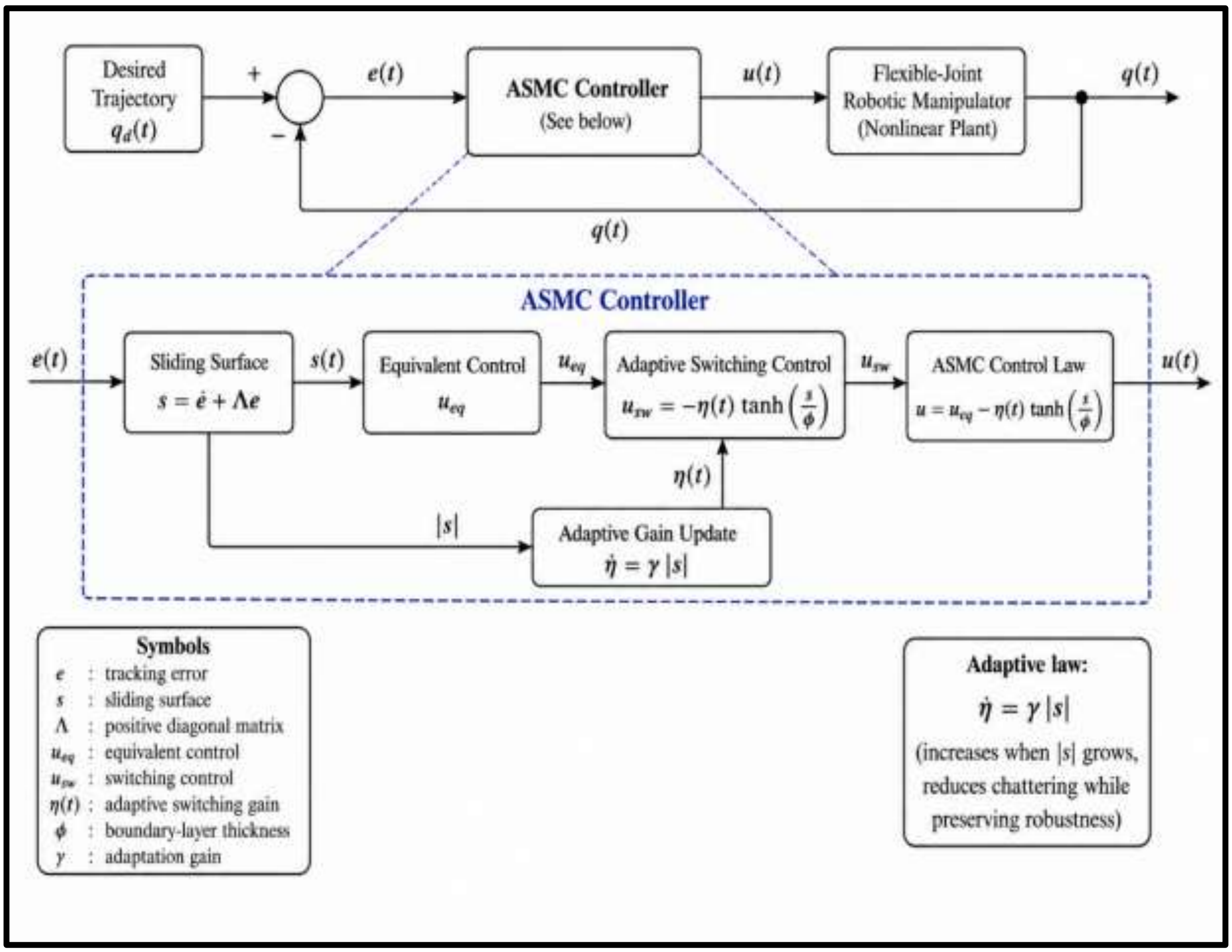


**Figure (4)** Block Diagram of the Proposed ASMC

### 2.3.2 Reinforcement Learning-Based Adaptive Sliding Mode Controller (RL-ASMC)

Although the ASMC provides robust position-tracking performance under nonlinear dynamics, payload variations, and external disturbances, its performance is influenced by the selection of the adaptive controller parameters. Therefore, a (RL-ASMC) is introduced to provide online tuning of the adaptive parameters according to the observed system behavior. In the proposed approach, reinforcement learning does not replace the ASMC structure; instead, it acts as an intelligent parameter-tuning mechanism for the underlying adaptive controller.

A Soft Actor-Critic (SAC) agent is employed because of its suitability for continuous action spaces. The agent receives information describing the instantaneous tracking behavior of the robotic manipulator. The state vector is defined as:

$st = [e(t), \dot{e}(t), S(t)]^T$ .......................... (24)

were e(t), ė(t), and), S(t) represent the position-tracking error, its time derivative, and the sliding variable, respectively.

The RL agent is used to tune the adaptive switching gain and its adaptation-rate parameter. Accordingly, the action vector is expressed as:

$at = [\eta t, \gamma t]^T$ .......................... (25)

where $\eta t$ is the adaptive switching gain and γt is the corresponding adaptation-rate parameter at time step $t$ . The sliding-surface parameter $\Lambda$ and $\boldsymbol{\varphi}$ the boundary-layer thickness are retained as fixed design parameters so that the fundamental ASMC structure is preserved.

The parameters supplied by the SAC agent are incorporated into the ASMC control law:

$u = u_{eq} - \eta(t) \tanh\left(\frac{S(t)}{\emptyset}\right)$ .......................... (26)

Thus, the RL agent continuously modifies the magnitude and adaptation rate of the switching action according to the instantaneous position-tracking behavior of the flexible-joint robotic manipulator.

The learning objective is formulated to simultaneously reduce the position-tracking error and avoid unnecessarily large control actions. The reward function is therefore defined as:

$Rt = -(we\, e^{\mathrm{T}}e + wu\, u^{\mathrm{T}}u)$ .......................... (27)

Here, **e** denotes the tracking error vector we want, **u** is the control input vector, and **we** and ***wu*** are positive weighting coefficients that are related to tracking error and control effort, respectively. This reward design, as such, incentivizes the RL agent to minimize tracking error while avoiding excessively large control activities thus enhancing both tracking precision and energy efficiency

Consequently, the proposed RL-ASMC combines the robustness of adaptive sliding mode control with the online parameter-optimization capability of reinforcement learning. This configuration enables the controller to adapt its switching behavior to variations in payload, nonlinear flexible-joint effects, and external disturbances while maintaining the basic ASMC control structure.

The overall architecture of the proposed RL-ASMC controller, including the interaction between the ASMC structure and the SAC-based adaptive parameter-tuning mechanism, is illustrated in figure 4.

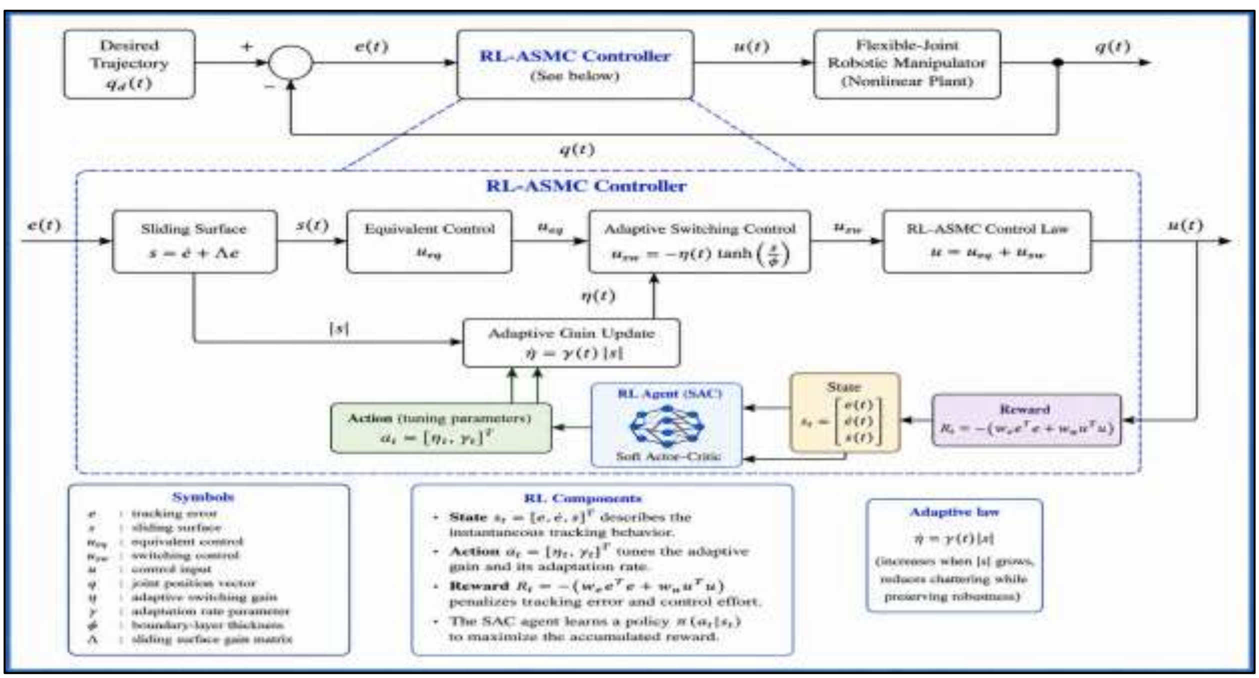


**Figure 4.** Block Diagram of the Proposed RL-ASMC Controller

## 3.Results and Discussion

The performance of the ASMC and RL-ASMC controllers was evaluated through both numerical simulation and experimental investigation to assess their position-tracking capability under different operating conditions. Two reference angles (45° and 135°) and three representative operating conditions, namely no-load condition, external disturbance, and 1000 g payload, were used in the tests for both controllers. To facilitate comparison, the same test conditions were established during the simulation and experimental investigations. Position tracking error, settling time and the estimated control torque were used as criteria for evaluating controller performance. The performance gain of the RL-ASMC with respect to the conventional ASMC was quantified and the validity of the results obtained from the simulation was compared with the results from the experiments.

**3.1 Simulation Results**

Numerical simulations were carried out with MATLAB/Simulink, based on the developed nonlinear dynamic model of the 4-DOF flexible-joint robotic manipulator. Both the ASMC and RL-ASMC controllers were designed and tested in the same manner for consistent comparison of their position tracking responses. The performance of both controllers is shown at the reference positions and operating conditions.

**3.1.1 ASMC Controller Simulation Results**

**1.Angle 45°**

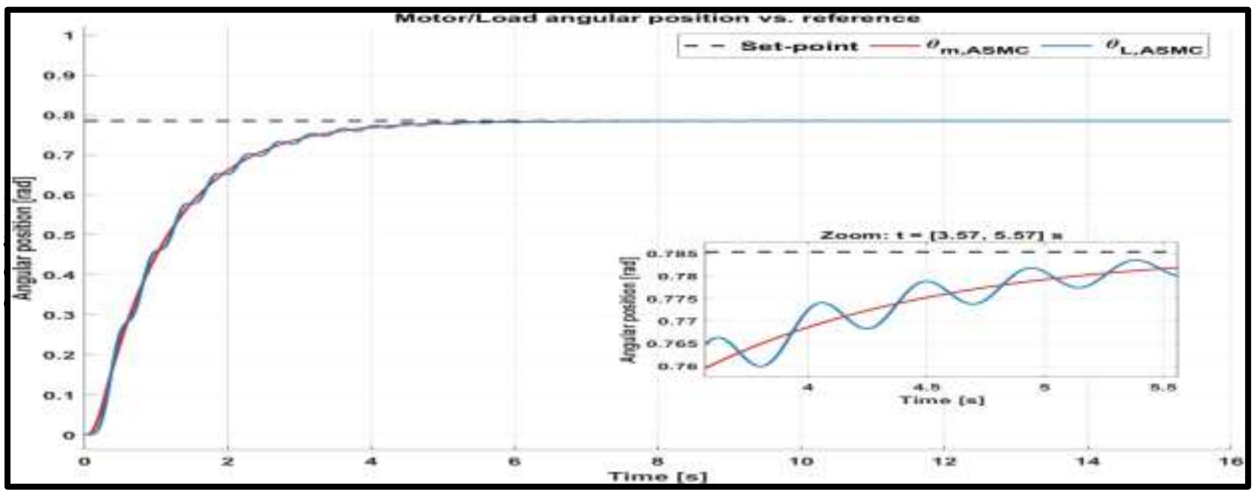


**Figure 5.** Simulated response of the ASMC controller under the no-load condition

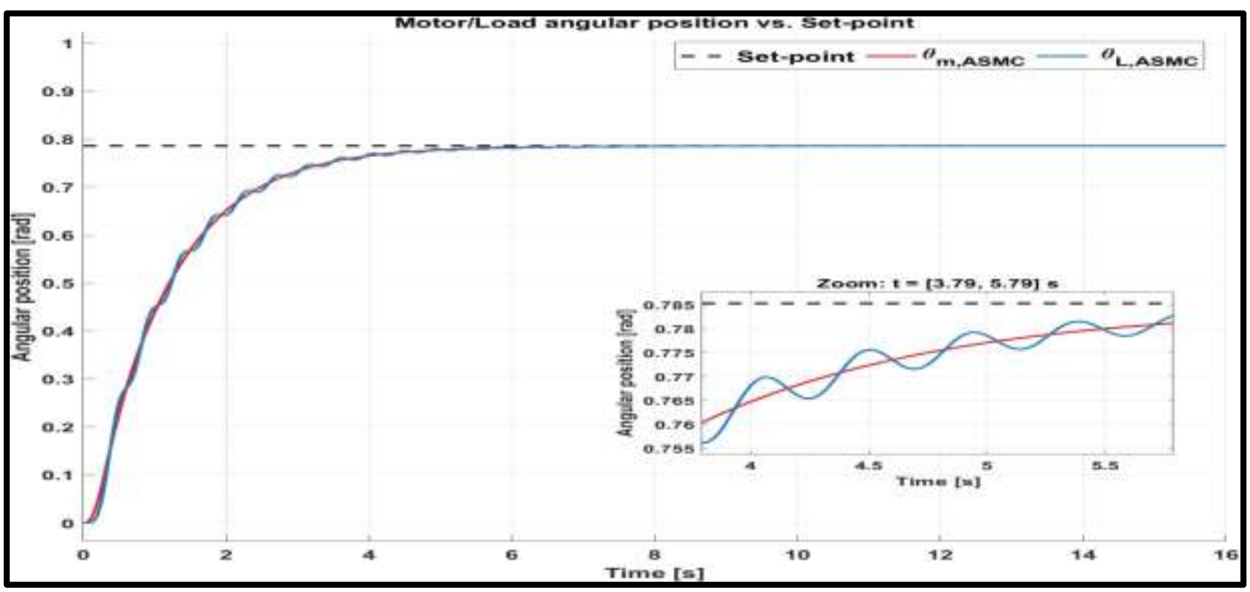


**Figure 6.** Simulated response of the ASMC controller under a 1000 g payload

Figure 6. illustrates the simulated response of the ASMC controller **under a 1000 g payload**. The controller maintained accurate tracking of the desired angular position despite the increased payload. The tracking error

rapidly converged to zero, while the estimated control torque remained smooth with only minor transient variations, demonstrating the adaptive capability of the ASMC controller to compensate for payload changes while preserving system stability.

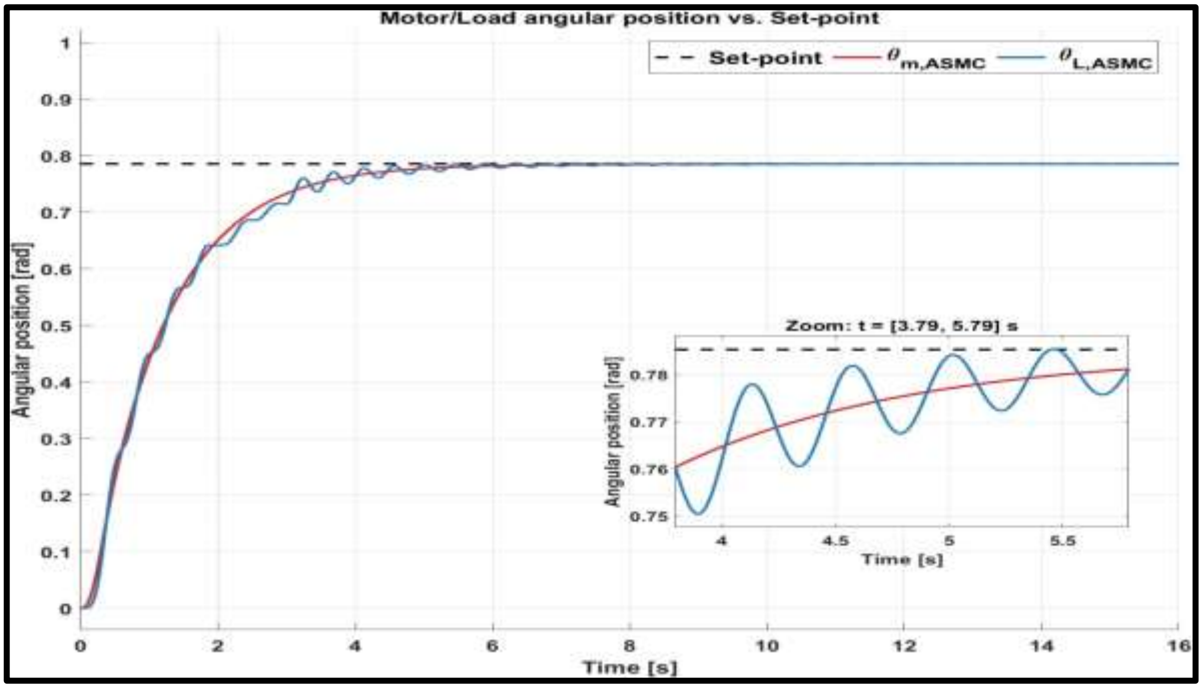


**Figure 7.** Simulated response of the ASMC controller under a 1000 g with external disturbance

Figure 7. illustrates the simulated response of the ASMC **controller under a 1000 g payload with an external disturbance.** The controller effectively compensated for the applied disturbance while maintaining accurate angular position tracking. Only slight transient variations were observed in the tracking error and estimated control torque immediately after the disturbance, after which the response quickly returned to the steady-state condition. These results demonstrate the improved adaptability and disturbance rejection capability of the ASMC controller compared with the conventional SMC controller.

**2.Angle (135°)**

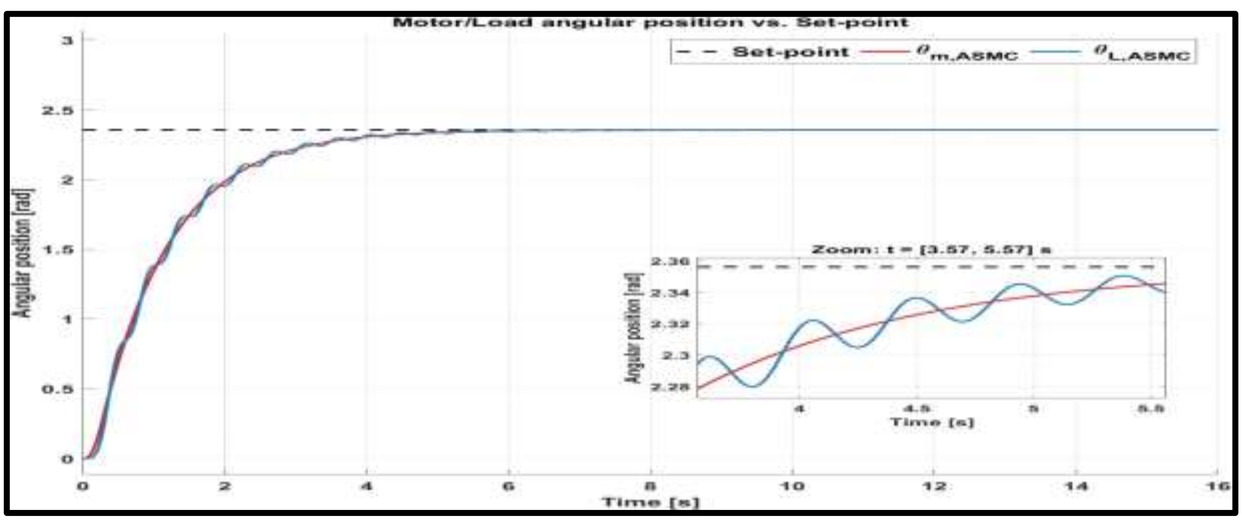


**Figure 8.** Simulated response of the ASMC controller under the no-load condition

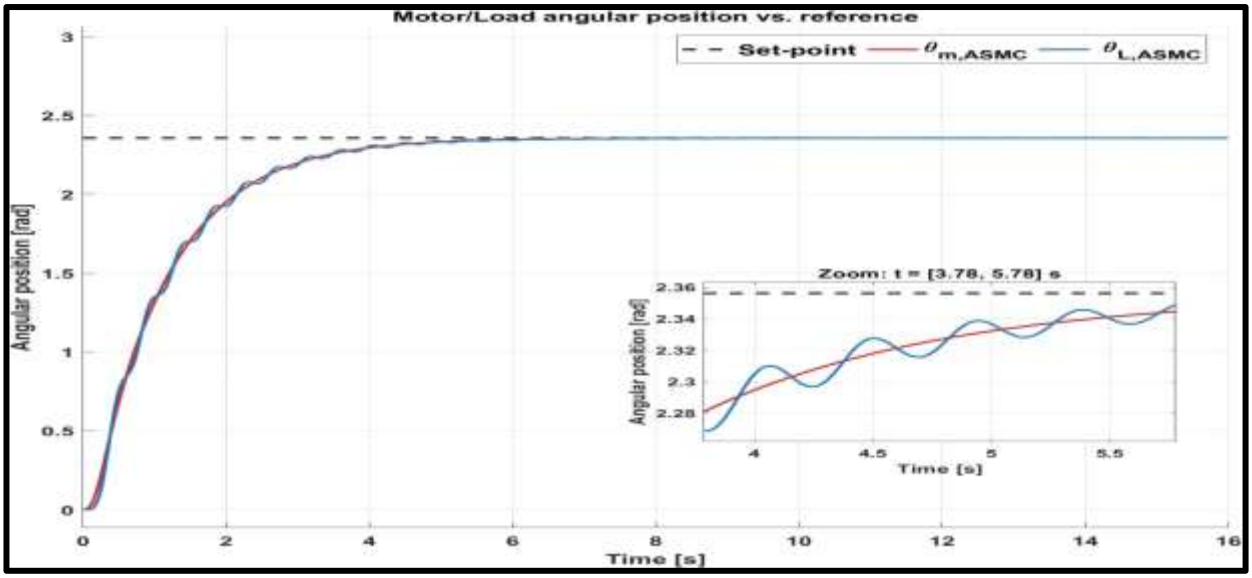


**Figure 9.** Simulated response of the ASMC controller under a 1000 g payload

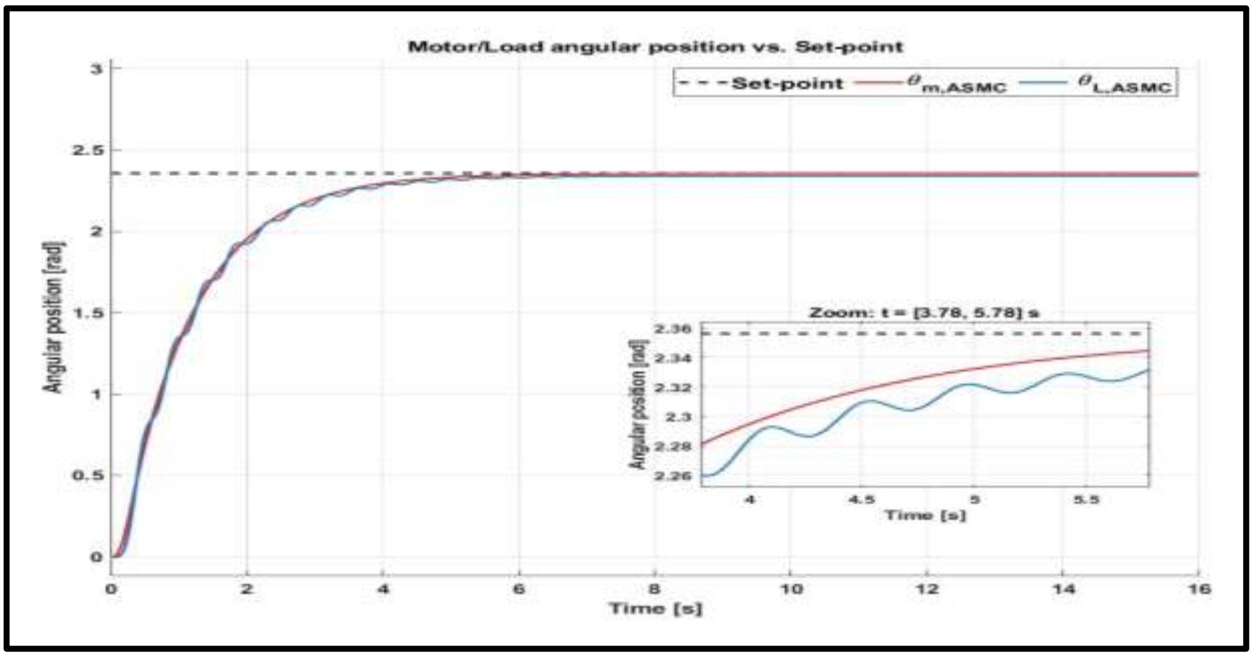


**Figure 10.** Simulated response of the ASMC controller under a 1000 g with external disturbance

The simulation performance of the ASMC controller was evaluated in Tables 1 and 2 summarize the obtained performance indices for reference angles of 45° and 135°, respectively.

**Table 1. Simulation performance indices of the ASMC controller at the 45° set point**

| Payload Condition | Average Estimated Torque (N·m) | Settling Time (s) | Simulation Angular Position Error (%) |
|---|---|---|---|
| **No Load** | **2.95** | **5.47** | **0.62** |
| **1000 g** | **3.16** | **5.57** | **0.78** |
| **External Disturbance** | **3.3** | **5.80** | **9.9** |

**Table 2. Simulation performance indices of the ASMC controller at the 135° set point**

| **Payload Condition** | **Average Estimated Torque (N·m)** | **Settling Time (s)** | **Simulation Angular Position Error (%)** |
|---|---|---|---|

| | | | |
|---|---|---|---|
| **No Load** | **4.1** | **5.6** | **0.48** |
| **1000 g** | **4.7** | **5.8** | **0.60** |
| **External Disturbance** | **5.1** | **6** | **0.81** |

### 3.1.2 RL-ASMC Controller Simulation Results

**1. Angle (45)**

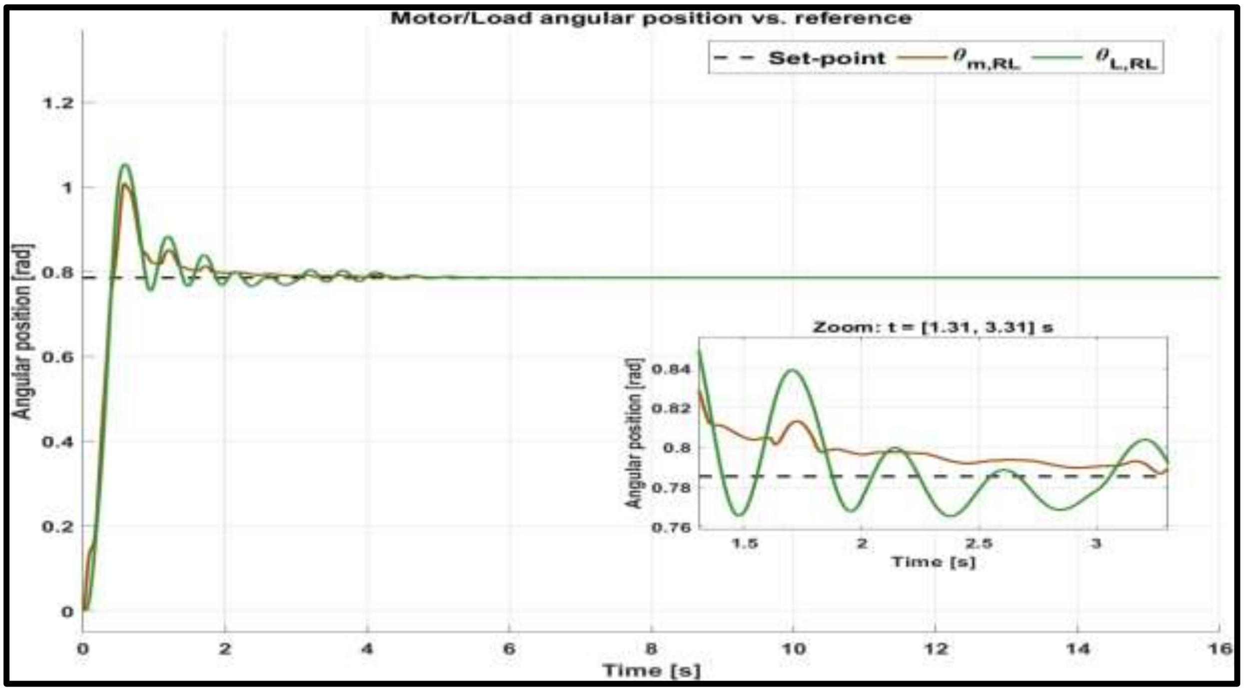


**Figure 11.** Simulated response of the (Rl-ASMC) controller under a 1000 g with external disturbance

Figure **11.** shows the simulated angular position response of the motor and load sides using the RL-ASMC controller at a 45° reference angle (0.785 rad). During the initial transient response, the load-side angular position reaches a maximum value of approximately 1.05 rad at about 0.6 s, corresponding to a maximum overshoot of approximately 34%. The subsequent oscillations progressively decay with time, and both the motor and load responses approach the desired position within approximately 5 s. The steady-state error becomes very small and approaches zero, indicating accurate and stable position tracking despite the initial oscillations caused by the flexible-joint dynamics.

**2.Angle (135)**

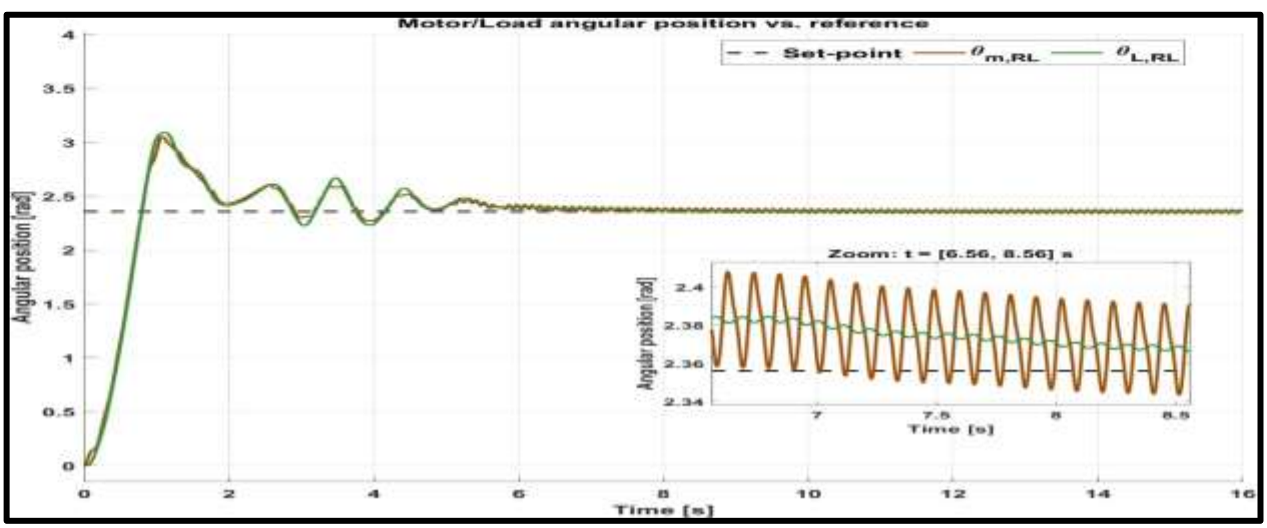


**Figure 12.** Simulated response of the (Rl-ASMC) controller under a 1000 g with external disturbance

Figure **12.** shows the simulated angular position response of the motor and load sides using the RL-ASMC controller at a 135° reference angle (2.356 rad). During the initial transient response, the angular position reaches a maximum value of approximately 3.10 rad at about 1.1 s, corresponding to a maximum overshoot of approximately 32%. The oscillations subsequently decrease as the system approaches the desired position, with the main transient response largely attenuated within approximately 5.54 s. The enlarged view between 6.56 and 8.56 s reveals small residual oscillations around the reference position, particularly on the motor side. Nevertheless, the steady-state error remains small, demonstrating stable and accurate position tracking at the higher reference angle.

It is noteworthy that, although the required angular displacement increased threefold from 45° to 135°, the system reached the steady-state region within approximately the same time range. This demonstrates the ability of the RL-ASMC controller to preserve a relatively consistent convergence performance even when the required angular displacement is significantly increased.

The simulation performance of the RL-ASMC controller was evaluated in Tables 3. and 4 summarize the obtained performance indices for reference angles of 45° and 135°, respectively.

**Table 3. Simulation performance indices of the RL-ASMC controller at the 45° set point**

| Payload Condition | Maximum Estimated Torque (N·m) | Settling Time (s) | Simulation Angular Position Error (%) |
|---|---|---|---|
| No Load | 2.15 | 4.33 | 0.163 |
| 1000 g | 2.46 | 4.46 | 0.278 |
| External Disturbance | 2.8 | 4.96 | 0.438 |

**Table 4. Simulation performance indices of the RL-ASMC controller at the 135° set point**

| Payload Condition | Maximum Estimated Torque (N·m) | Settling Time (s) | Simulation Angular Position Error (%) |
|---|---|---|---|
| No Load | 014 | 4.31 | 0.14 |
| 1000 g | 1.18 | 4.7 | 0.192 |
| External Disturbance | 1.235 | 5.14 | 0.235 |

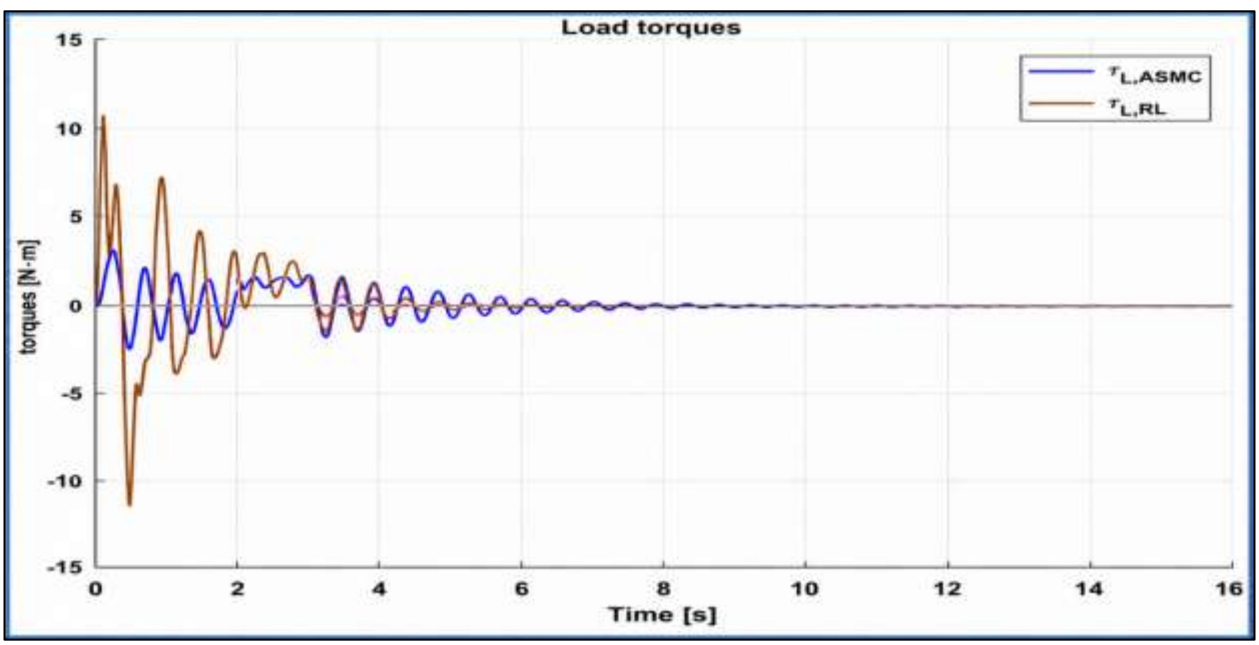


**Figure 5.30:** Load torque response of two controllers under external disturbance (45°)

### 3.2 Experimental Results

The practical performance of the ASMC and RL-ASMC controllers was validated by experiments on a fabricated 4-DOF flexible-joint robotic manipulator. The controllers were real-time programmed using LabVIEW and NI myRIO and angular responses and control variables were measured directly from the experimental platform. The experimental tests were conducted in the same reference positions and operating conditions used in the simulation and so could be compared consistently to the simulation. The results are evaluated in terms of position-tracking error, settling time, and estimated control torque, with particular emphasis on the practical improvement achieved by the RL-ASMC over the ASMC.

**3.2.1 Experimental Results of (ASMC)**

**1. 45° No load**

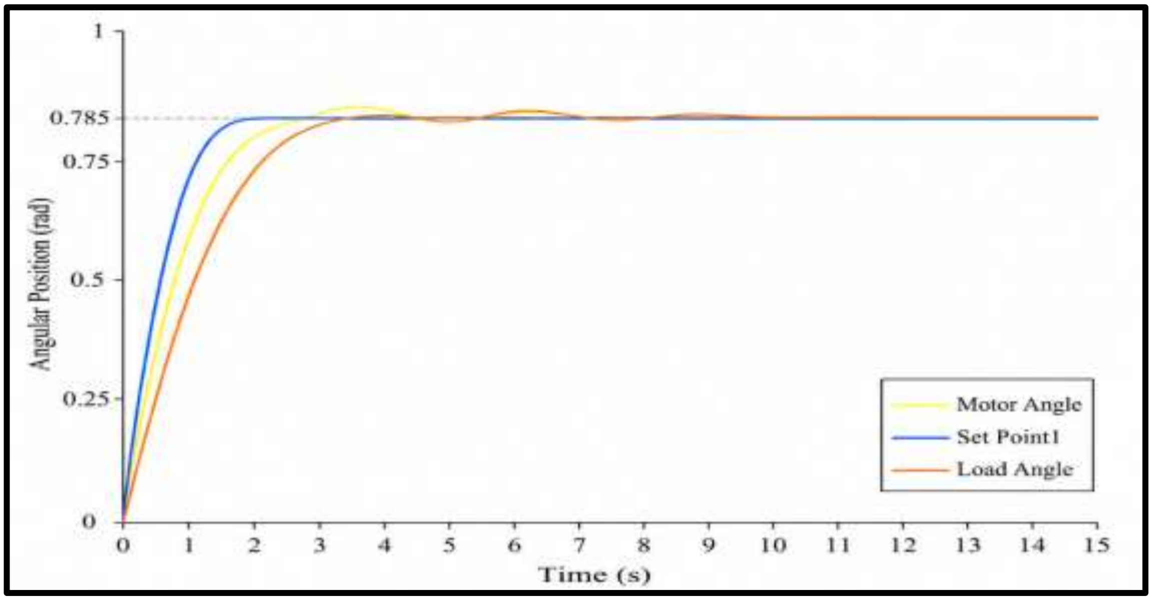


**Figure 13.** Experimental response of the ASMC under the no-load condition

**2. (1000 g Payload)**

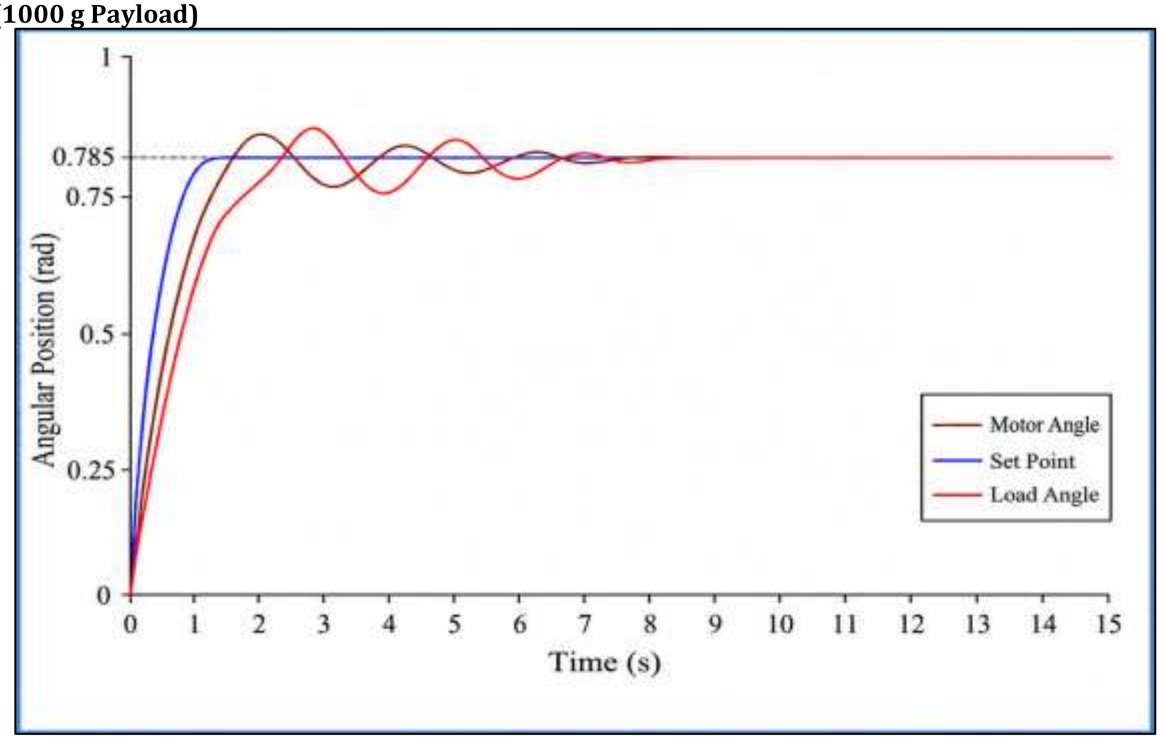


**Figure 14.** Motor, load, and set-point response positions under 1000g

**3. (1000 g Payload with External Disturbance)**

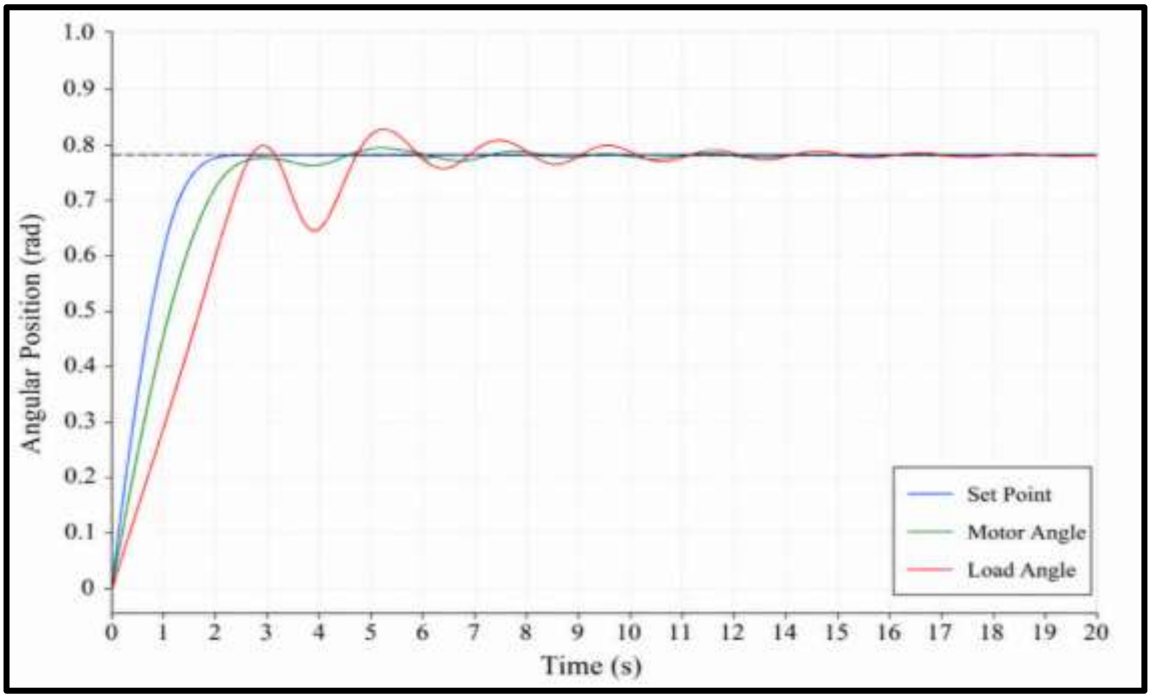


**Figure 15.** Experimental response of the ASMC with 1000 g and an external disturbance

**3.2.2 Experimental Results of (RL-ASMC)**
**1.No-Load Condition with Set Point 45°**

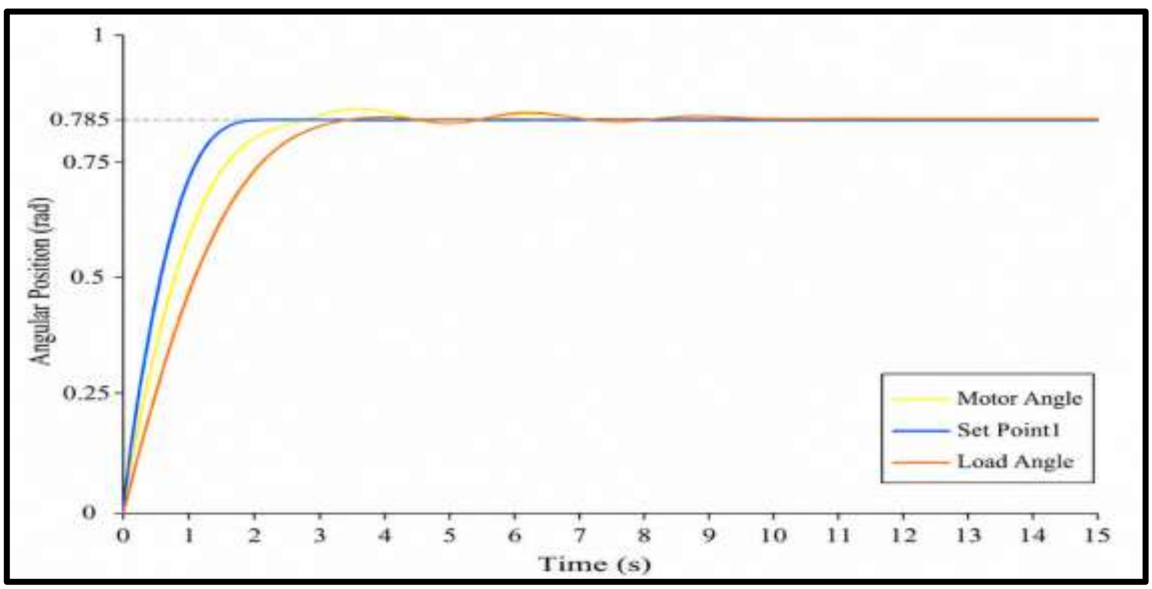


**Figure 16.** Experimental response of the ASMC under the no-load condition

1. (1000 g Payload)

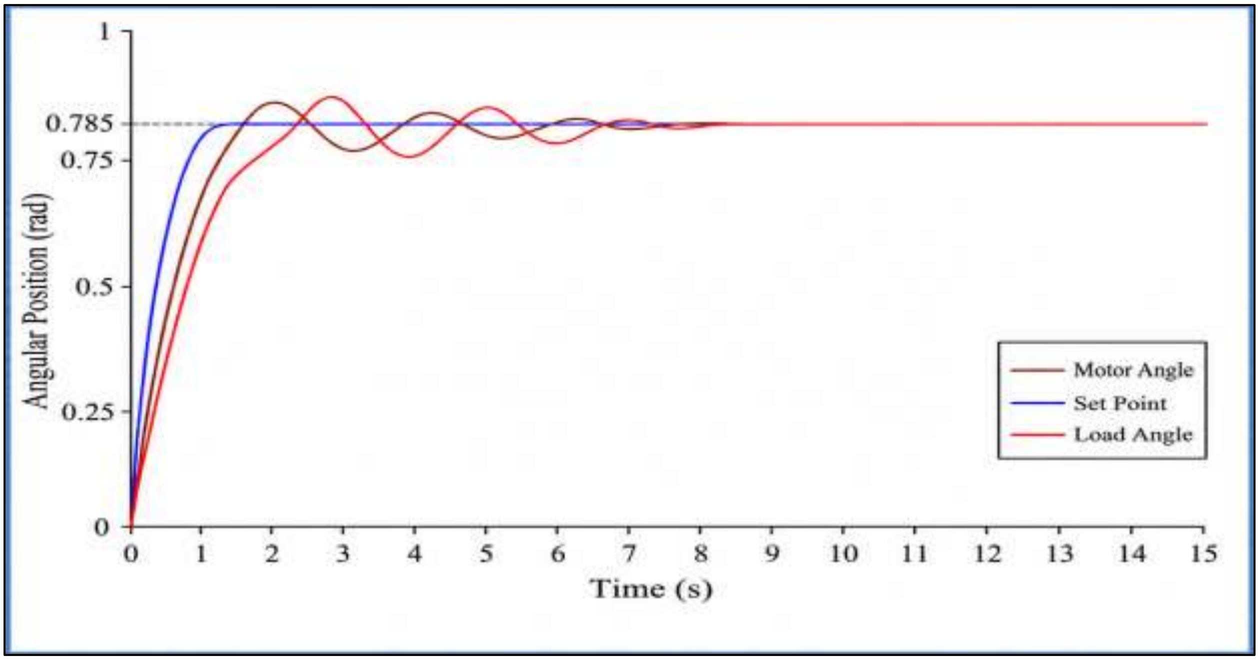


**Figure 17.** Motor, load, and set-point response positions under 1000g

3. (1000 g Payload with External Disturbance)

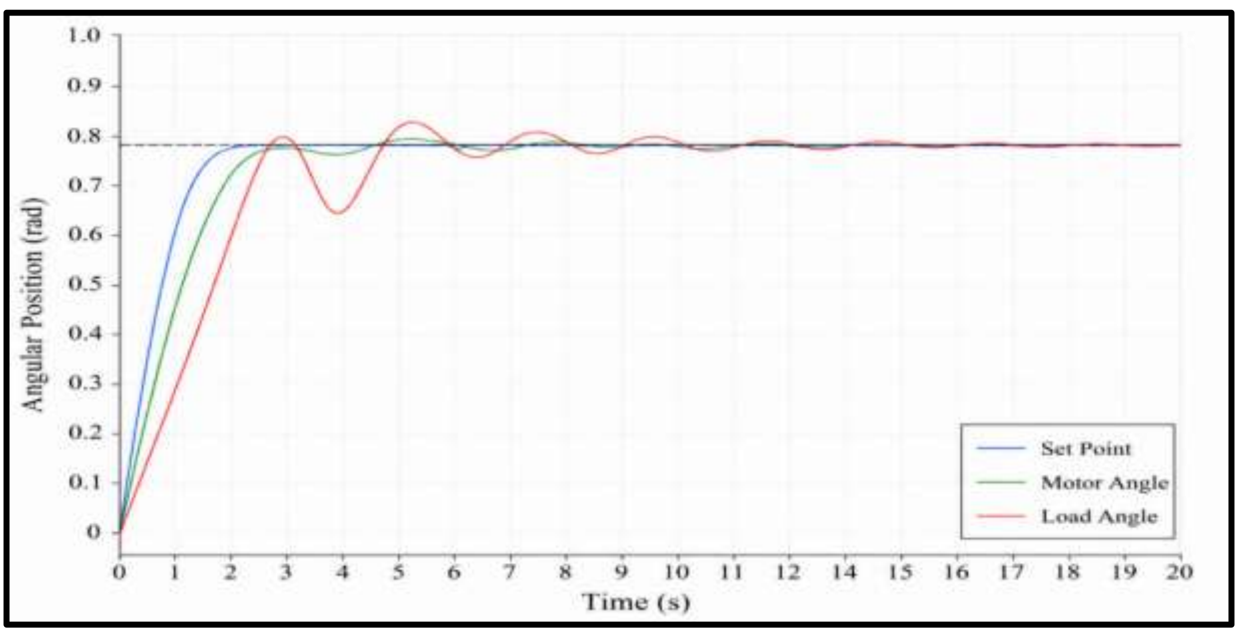


**Figure 18.** Experimental response of the ASMC with 1000 g and an external disturbance

## 4. Conclusions

Based on the simulation and experimental investigations, the main conclusions of this study can be summarized as follows:

1. A 4-DOF flexible-joint robotic manipulator incorporating a fabricated four-spring flexible-joint mechanism was successfully developed, mathematically modeled, and experimentally implemented.

2. Both ASMC and RL-ASMC achieved stable position tracking at the reference angular positions of 45° and 135° under no-load, 1000 g payload, and external-disturbance conditions.
3. The proposed RL-ASMC significantly improved angular position accuracy compared with ASMC. The average experimental angular position error decreased from approximately 0.85% with ASMC to 0.25% with RL-ASMC, corresponding to an improvement of approximately 70.6%.
4. The average settling time was reduced from approximately 5.4 s for ASMC to 4.2 s for RL-ASMC**, representing an improvement of approximately 22.2%. This demonstrates the faster convergence of RL-ASMC toward the desired angular position.
5. The average estimated control torque decreased from approximately 3.1 N·m with ASMC to 2.5 N·m with RL-ASMC, corresponding to a reduction of approximately 19.4%. Thus, the improved position tracking and response speed were achieved with reduced control effort.
6. The performance improvements of RL-ASMC were maintained under payload variation and external disturbance, demonstrating greater adaptability and robustness than the conventional ASMC.
7. The simulation and experimental studies demonstrated the same trends of performance. Overall, RL-ASMC showed an average reduction of about 70.6% in the angular position error, 22.2% in settling time, and 19.4% in estimated control torque compared to ASMC.
8. The results demonstrate the effectiveness of the proposed RL-ASMC in improving the position accuracy, response speed, and control efficiency of the developed flexible-joint robotic manipulator.
The SAC-based reinforcement-learning agent effectively tuned the adaptive parameters ($\eta$) and ($\gamma$) while preserving the underlying ASMC structure.

**6. Recommendations and Future Work**

1. The proposed RL-ASMC can be extended to control multiple flexible joints simultaneously and evaluated on robotic manipulators with higher degrees of freedom.
2. Future studies can investigate the performance of other reinforcement learning algorithms and compare them with the SAC-based approach used in this study.
3. The proposed controller can be evaluated under wider operating conditions, including different payloads, continuous trajectories, and various types of external disturbances.
4. Future work can focus on real-time optimization of additional controller parameters and investigate the implementation of RL-ASMC in more complex industrial robotic applications.

## References

[1] Tuan, H. M., Sanfilippo, F., and Hao, N. V., "Modelling and control of a 2-DOF robot arm with elastic joints for safe human–robot interaction," Frontiers in Robotics and AI, vol. 8, 2021.
[2] Ma, H., Zhou, Q., Li, H., and Lu, R., "Adaptive prescribed performance control of a flexible-joint robotic manipulator with dynamic uncertainties," IEEE Transactions on Cybernetics, vol. 52, pp. 12905–12915, 2022.
[3] Xu, X. and Xu, S., "Event-triggered adaptive neural tracking control of flexible-joint robot systems with input saturation," IEEE Access, vol. 10, pp. 43367–43375, 2022.
[4] Shang, D., Li, X., Yin, M., and Li, F., "Dynamic modeling and fuzzy adaptive control strategy for space flexible robotic arm considering joint flexibility based on improved sliding mode controller," Advances in Space Research, vol. 70, no. 10, pp. 3093–3106, 2022.
[5] Meng, X., Hu, J., Wang, P., and Zhao, S., "Passivity-based control for flexible-joint robots with vibration suppression and input constraints," Journal of the Franklin Institute, vol. 360, no. 12, pp. 8542–8565, 2023.
[6] Iskandar, M., van Ommeren, C., Wu, X., Albu-Schäffer, A., and Dietrich, A., "Model predictive control applied to different time-scale dynamics of flexible joint robots," IEEE Robotics and Automation Letters, vol. 8, pp. 672–679, 2023.
[7] Moyrón, J., Moreno-Valenzuela, J., and Sandoval, J., "Nonlinear PI 'D'-type control of flexible joint robots by using motor position measurements is globally asymptotically stable," IEEE Transactions on Automatic Control, vol. 68, pp. 3648–3655, 2023.
[8] Zhu, Y., Liu, J., Yu, J., and Wang, Q. G., "Command filtering-based adaptive fuzzy control of flexible-joint robots with time-varying full-state constraints," IEEE Transactions on Circuits and Systems II: Express Briefs, vol. 71, pp. 682–686, 2024.
[9] Rsetam, K., Cao, Z., and Man, Z., "Design of robust terminal sliding mode control for underactuated flexible joint robot," IEEE Transactions on Systems, Man, and Cybernetics: Systems, vol. 52, 2022.
[10] Cheng, X., Liu, H., and Lu, W., "Chattering-suppressed sliding mode control for flexible-joint robot manipulators," Actuators, vol. 10, art. 288, 2021.

[11] Zaare, S. and Soltanpour, M. R., "Adaptive fuzzy global coupled nonsingular fast terminal sliding mode control of n-rigid-link elastic-joint robot manipulators in presence of uncertainties," Mechanical Systems and Signal Processing, vol. 163, art. 108165, 2022.

[12] Mohammad, A. M., Al-Samarraie, S. A., and Jaber, A. A., "Barrier Function-Based Integral Sliding Mode Controller Design for a Single-Link Rotary Flexible Joint Robot," International Journal on Smart Sensing and Intelligent Systems, vol. 17, no. 1, 2024.

[13] Nezhad, A. H., Noiey, A. R., Soltanpour, M. R., and Veysi, M., "A new fuzzy decoupled sliding mode control of flexible joint robotic manipulators based on the finite-time observer in the presence of chaos with experimental validation," IET Control Theory & Applications, vol. 18, pp. 422–441, 2024.

[14] Li, J., Ma, K., and Wu, Z., "Prescribed performance control for uncertain flexible-joint robotic manipulators driven by DC motors," International Journal of Control, Automation and Systems, vol. 19, pp. 1640–1650, 2021.

[15] Chen, H. Y., Dong, X. C., Yang, Y., and Liu, J. T., "Fixed-time tracking control for flexible joint manipulator with prescribed performance constraint," IEEE Access, vol. 9, pp. 99388–99397, 2021.

[16] Phan, V. D., Vo, C. P., and Ahn, K. K., "Adaptive neural tracking control for flexible joint robot including hydraulic actuator dynamics with disturbance observer," International Journal of Robust and Nonlinear Control, vol. 34, no. 13, pp. 8744–8767, 2024.

[17] Al-Ashtari, W. and Ali, K. H., "Design of a Hybrid Adaptive Controller for Series Elastic Actuators of Robots," Journal Européen des Systèmes Automatisés, vol. 56, no. 6, pp. 1059–1068, 2023.

[18] Zotovic-Stanisic, R., Perez-Ubeda, R., and Perles, A., "Comparative Study of Methods for Robot Control with Flexible Joints," Actuators, vol. 13, no. 8, art. 299, 2024.

[19] Cao, S., Wang, F., Li, X., Yao, D., and Xie, M., "Safety-Constrained Disturbance-Compensated Model Predictive Control for Flexible-Joint Robots," Applied Sciences, 2025.

[20] Sutton, R. S. and Barto, A. G., Reinforcement Learning: An Introduction, 2nd ed., MIT Press, 2018.

[21] Kiumarsi, B., Vamvoudakis, K. G., Modares, H., and Lewis, F. L., "Optimal and autonomous control using reinforcement learning: A survey," IEEE Transactions on Neural Networks and Learning Systems, vol. 29, no. 6, pp. 2042–2062, 2018.

[22] Pavlichenko, D. and Behnke, S., "Real-Robot Deep Reinforcement Learning: Improving Trajectory Tracking of Flexible-Joint Manipulator with Reference Correction," 2022.

[23] Zhong, H., Wen, W., Fan, J., and Yang, W., "Reinforcement learning-based adaptive tracking control for flexible-joint robotic manipulators," AIMS Mathematics, vol. 9, no. 10, pp. 27330–27360, 2024.

[24] Li, X., Zheng, D., Guo, K., and Ren, X., "Identification and Control of Flexible Joint Robots Based on a Composite-Learning Optimal Bounded Ellipsoid Algorithm and Prescribe Performance Control Technique," Applied Sciences, vol. 14, no. 10, art. 4030, 2024. DOI: 10.3390/app14104030.

[25] Zhang, Z., Hu, X., and Huang, P., "Disturbance Observer-Based Tracking Controller for n-Link Flexible-Joint Robots Subject to Time-Varying State Constraints," Electronics, vol. 13, no. 9, art. 1773, 2024. DOI: 10.3390/electronics13091773.

[26] Moyrón, J., Ott, C. D., Kirner, A., and Moreno-Valenzuela, J., "Elastic Structure Preserving Control for Flexible Joint Robots With Position-Controlled Actuators," IEEE Transactions on Control Systems Technology, vol. 33, no. 5, pp. 1810–1819, 2025. DOI: 10.1109/TCST.2025.3562024.

[27] Cao, S., Wang, F., Li, X., Yao, D., and Xie, M., "Safety-Constrained Disturbance-Compensated Model Predictive Control for Flexible-Joint Robots," Applied Sciences, vol. 15, no. 24, art. 13238, 2025. DOI: 10.3390/app152413238.

[28] S.K. Hasan and Anoop K. Dhingra, " Development of a sliding mode controller with chattering suppressor for human lower extremity exoskeleton robot," Results in Control and Optimization, vol. 7, no. 100123, 2022.